China Geology 9 (2026) 456−467

China Geology

Journal homepage: http://chinageology.cgs.cn
https://www.sciencedirect.com/journal/china-geology

Dynamic accumulation of gas hydrates in the Shenhu area, northern South China Sea: A two-stage evolution model constrained by temporally varying fluid flow

Zheng Su[a, b,*], Yi-fan Wu[a, b,*], Neng-you Wu[c, d]

[a] *Guangzhou Institute of Energy Conversion*, *Chinese Academy of Sciences*, *Guangzhou* 510640, *China*
[b] *School of Energy Science and Engineering*, *University of Science and Technology of China*, *Guangzhou* 510640, *China*
[c] *Key Laboratory of Gas Hydrate*, *Ministry of Natural Resources*, *Qingdao Institute of Marine Geology*, *Qingdao* 266237, *China*
[d] *Laoshan Laboratory*, *Qingdao* 266200, *China*

A R T I C L E I N F O

Article history:
Received 22 July 2025
Received in revised form 22 October 2025
Accepted 25 November 2025
Available online 25 February 2026

Keywords:
Gas hydrate
Combustible ice
Clean energy
Shenhu area
Pleistocene sediments
Water flow rate
Sedimentation rate
Tectonic activity
Numerical modeling

A B S T R A C T

Gas hydrates occurring within the Pleistocene sediments of the Shenhu area, South China Sea, represent a dynamically evolving accumulation inherited from an "ancient" hydrate system. A hydrate-enriched layer with a maximum saturation of 48% is present near the base of the current gas-hydrate stability zone (GHSZ), above which hydrate saturation rapidly declines to nearly zero. This sharp transition cannot be explained by the previously estimated slow and nearly constant aqueous flow rate for the Pleistocene sediments. Geological evidence indicates that a substantial reduction in fluid flow occurred during the Early Pleistocene. To explore this process, the authors develop a coupled fluid–heat flow numerical model to simulate the dynamic evolution of the Shenhu hydrate system under temporally varying water-flow conditions. The model incorporates both the burial of "ancient" hydrates through sedimentation and the formation of "new" hydrates in younger deposits. Simulations with time-dependent flow rates can successfully reproduce the observed hydrate distribution in the Shenhu area. Under present sedimentation and fluid-flow conditions, the burial and dissociation of "ancient" hydrates beneath the GHSZ greatly outpace the formation of "new" hydrates within it, resulting in a continuous decline in the total hydrate inventory over time. These findings offer new insights into the long-term evolution of natural hydrate systems and have important implications for *in-situ* hydrate resource assessment.

©2026 China Geology Editorial Office.

1. Introduction

Gas hydrates are ice-like crystalline substances that occur in nature when solid water lattices encapsulate gas molecules within cage-like structures (Sloan ED and Koh CA, 2008). They form under conditions of relatively high pressure and low temperature, such as those found in the shallow subsurface beneath many of the world's deep-water oceans. The volume of natural gas stored in methane hydrates worldwide is estimated to be far greater than that contained in all conventional natural-gas resources (Milkov A, 2004; Piñero E et al., 2012).

Because of their potential significance as an energy resource (Collett T, 2002), a greenhouse-gas source (Biastoch A et al., 2011; Lunt D et al., 2011), a component of the global carbon cycle (Dickens G, 2003), and a trigger of marine geologic hazards (Sultan N et al., 2004), natural gas hydrates have been extensively investigated worldwide. Understanding how hydrates accumulate in marine sediments over time is essential (Bhatnagar G et al., 2007), and numerical modeling has proven to be an effective tool for this purpose (Xu WY and Ruppel C, 1999; Davie M and Buffett B, 2001; Bhatnagar G et al., 2007; Zhu LQ et al., 2022).

Gas hydrates have been identified on the northern continental slope of the South China Sea (SCS) through geological, seismic, geochemical, and biological evidence, where they represent a significant potential gas resource (Wu NY et al., 2009). The Shenhu area is one of the most promising targets in China (Fig. 1). A breakthrough came with the GMGS-1 drilling expedition conducted by the Guangzhou Marine Geological Survey, which recovered

First author: *E-mail address*: suzheng@ms.giec.ac.cn (Zheng Su).

* Corresponding author: *E-mail address*: suzheng@ms.giec.ac.cn (Zheng Su); wyf0924@mail.ustc.edu.cn (Yi-fan Wu).

Literary editor: Jie Meng
doi:10.31035/cg2025196
2096-5192/© 2026 China Geology Editorial Office.

Copyright © 2026 Editorial Office of China Geology. Publishing services by Elsevier B.V. on behalf of KeAi Communications Co. Ltd.
This is an open access article under the CC BY-NC-ND License (http://creativecommons.org/licenses/by-nc-nd/4.0/).

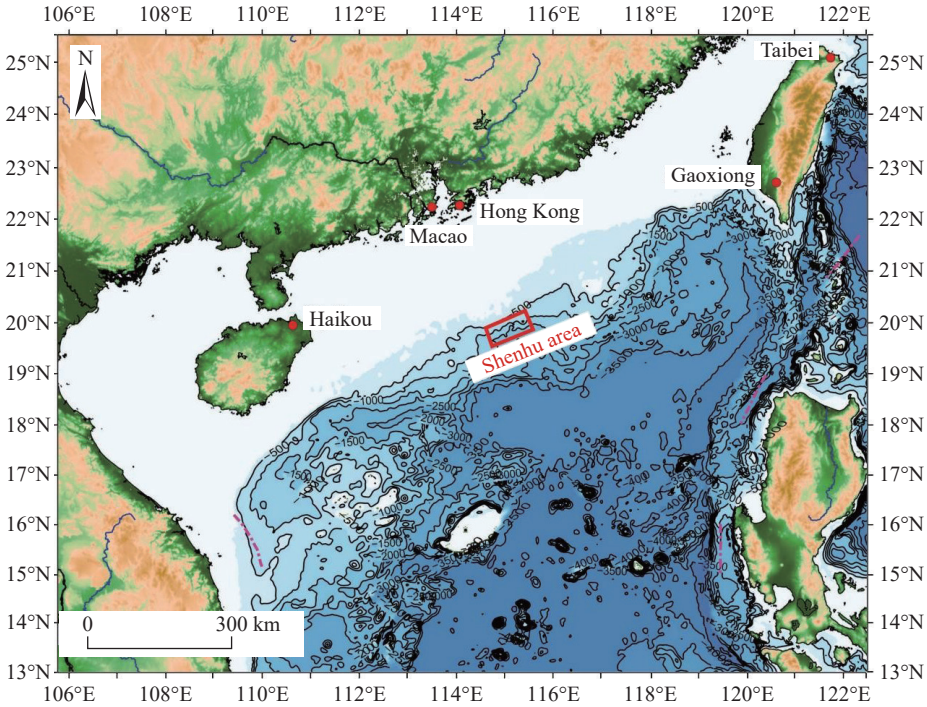

Fig. 1. Location of Shenhu area on the northern continental slope of the South China Sea. Red dashed lines denote marine administrative boundaries of China (schematic). The Shenhu area (red box) marks the general region of the GMGS-1 drilling sites, including site SH2 examined in this study.

hydrate-bearing cores from three sites in water depths of 1108–1235 m (Zhang HQ et al., 2007). These cores revealed high hydrate saturation in clay-rich silt sediments, with methane as the dominant gas component (Zhang HQ et al., 2007; Wu NY et al., 2008, 2010; Zhu LQ et al., 2023c, 2023d).

Seismic data further show that the Shenhu sediments are cut by a series of NE-trending fracture zones and a distinct bottom-simulating reflector (BSR), which indicate active fluid-migration pathways and a close association between tectonic deformation and hydrate occurrence (Fig. 2; Wu NY et al., 2009; Su Z et al., 2012). These structural conduits likely enhanced upward fluid flow and methane transport during past tectonic episodes, providing favorable conditions for hydrate formation.

This study estimated hydrate saturation (S_h, the fraction of pore volume occupied by hydrate) at site SH2 using measured pore-water salinity and resistivity logs. Hydrates are concentrated within a 22-m-thick layer (S_h > 20%) near the base of the present-day gas-hydrate stability zone (GHSZ, 229 mbsf), where the maximum saturation reaches about 48% at 204 mbsf. Hydrate saturation decreases sharply upward to nearly zero—quite different from the smoother distributions predicted by earlier numerical models (Davie M and Buffett B, 2001, 2003; Xu WY, 2004; Bhatnagar G et al., 2007; Zhu LQ et al., 2023a, 2023b).

Previous numerical modeling studies (Guan JA et al., 2009; He LJ et al., 2011) have attributed hydrate accumulation either to free-gas migration through highly permeable sediments or to focused seepage associated with mud volcanoes and gas chimneys. However, the absence of

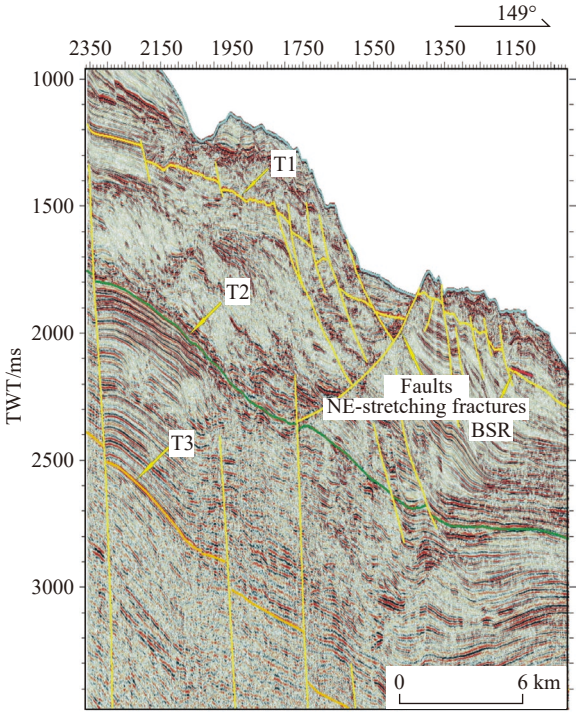

Fig. 2. Seismic profile HS623 showing NE-trending fractures and bottom-simulating reflector (BSR) in the Shenhu area, northern South China Sea. Two sets of oppositely dipping fracture zones indicate active fluid-migration pathways in the sediments (after Wu NY et al., 2009; Su Z et al., 2012). The top horizontal axis denotes the common-depth-point (CDP) number along the profile, 149° indicates the profile azimuth, and the vertical axis (TWT/ms) is the two-way travel time in milliseconds. T1, T2, and T3 are major seismic reflection interfaces (regional sequence boundaries) within the sediments.

abundant carbonate nodules and other petrographic indicators of active seepage suggests that free-gas migration was limited in the Shenhu area.

Many subsequent studies (Su Z et al., 2012; Fang YX et al., 2019; Chen C et al., 2020; Zhang W et al., 2020; Jin JP et al., 2020; Hu GW et al., 2021) have shown that hydrate accumulation on the northern South China Sea margin depends primarily on the methane-supply rate within thick sedimentary layers and that sedimentation rate strongly influences the spatial distribution of hydrate content. Gas chimneys and faults provide vertical pathways for methane migration (Chen C et al., 2020), and the coupling of gas supply with multiple migration routes produces highly saturated hydrate zones (Zhang W et al., 2020). High hydrate saturation and anomalous pore-water chlorinity at Shenhu area indicate upward methane transport into the GHSZ (Jin JP et al., 2020), and the hydrate formation rate correlates positively with chloride concentration (Fang YX et al., 2019).

Su Z et al. (2012) proposed that hydrate distribution and evolution may be controlled by temporal variations in water-flow rate. Their study suggested an average sedimentation rate of 16 cm/ka and a present-day water-flow rate of 0.7 m/ka at site SH2, but modeling with these parameters could not reproduce the observed hydrate saturations. Hence, the authors hypothesize that fluid flow has varied over time due to tectonic activity and that the hydrates currently observed at Shenhu area originated from an ancient hydrate system formed in faulted sediments under higher flow rates and methane supply.

This study postulate that hydrate accumulation in the Shenhu sediments is strongly influenced by variations in seafloor sedimentation and water-flow rates. A clearer understanding of the system's dynamic evolution is needed to assess how regional sedimentation history and tectonic processes affect fluid flow. In this study, the authors first describe the regional geological setting of the Shenhu area and then use a time-dependent numerical model to illustrate the dynamic evolution of hydrate accumulation. The model quantifies key parameters controlling hydrate formation and elucidates the role of geological activity in shaping the hydrate system.

The novelty of this work lies in linking the modern hydrate system to a hypothesized ancient hydrate system developed under tectonically enhanced fluid-flow conditions. The conceptual differences between the two systems are schematically illustrated in Fig. 3. The ancient system (>1.5 Ma) featured fractured, high-permeability sediments and rapid advective methane transport, whereas the modern system (<1.5 Ma) formed after tectonic quiescence, with fine-grained, low-permeability sediments and much slower flow.

Against this background, this study aims to explore the dynamic evolution of gas hydrate accumulation in the Shenhu area by integrating regional sedimentation history, tectonic activity, and fluid-flow processes. A time-dependent numerical model constrained by geological and geochemical observations at site SH2 is employed to investigate how variations in sedimentation and water-flow rates influence

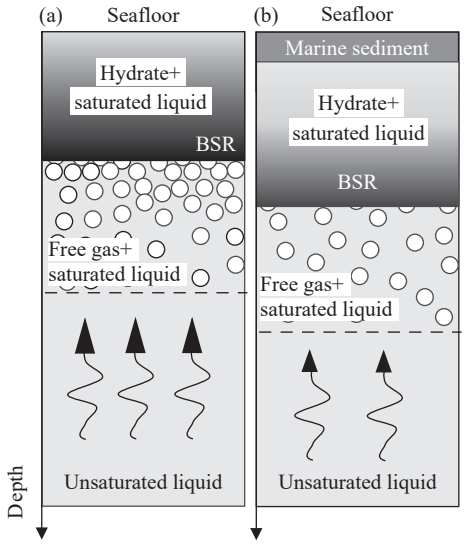

Fig. 3. Conceptual comparison between the ancient and modern hydrate systems in the Shenhu area (after Haacke R et al., 2008). a–Ancient hydrate system (>1.5 Ma): Developed in fractured, high-permeability sediments under rapid fluid flow and active methane supply; b–modern hydrate system (<1.5 Ma): Formed in fine-grained, low-permeability sediments under slow advective flow after tectonic quiescence. The schematic illustrates the contrasting fluid-migration intensity, hydrate occurrence, and free-gas distribution between the two stages.

hydrate formation and redistribution. Particular attention is paid to the potential linkage between the present-day hydrate system and a hypothesized ancient hydrate system developed under tectonically enhanced fluid-flow conditions. The results are expected to improve the understanding of hydrate accumulation mechanisms on the northern South China Sea margin and provide implications for similar continental-margin hydrate systems.

2. Geological setting

The Shenhu area is located in the Pearl River Mouth Basin and has been undergoing subsidence since the Miocene. The average sedimentation rate during this period has remained relatively high (approximately 160 m/Ma). The organic matter content in the sediments ranges from 0.2% to 1.9% (McDonnell S et al., 2000; Prell W et al., 2000; Wu NY et al., 2009); it is very low at shallow depths and relatively higher in deeper layers (Prell W et al., 2000). The sediments at the drilling sites in the Shenhu area mainly consist of muddy silt or silty mud (Su Z et al., 2012).

The low organic-matter content suggests that the contribution of *in-situ* biogenic methane to hydrate formation in the shallow sediments is very limited. Therefore, most of the methane in the gas hydrates was likely transported upward from deeper sources in the aqueous phase by advection and diffusion. The fine-grained sediments in the shallow section imply a low aqueous-flow rate. Moreover, the presence of only a few seep-carbonate nodules in the sediments indicates that there has been no significant free-gas leakage over geological time.

The deeper sediments below the present-day hydrate

accumulation in the Shenhu area are reported to be highly fractured and faulted due to four major tectonic events spanning from the Early Cretaceous to the Early Pleistocene. The faulting activity culminated around 1.5–2.0 Ma. The hydrates are currently accumulated within Pleistocene sediments (about 1.5 Ma; Wu NY et al., 2009; Kuang ZG and Guo YQ, 2011). Seismic data also reveal large-scale, deep-seated mud diapirs that penetrate the shallow sediments (Wu NY et al., 2009). These observed faults and mud diapirs likely represent paleo–fluid-flow conduits that transported methane from deeper sources into the hydrate stability field.

Past tectonic activities rendered the sediments highly permeable. The fractured layers and fault channels facilitated vigorous upward fluid flow toward the seafloor during these periods (Wu NY et al., 2009). Gas hydrates could have developed in the sediments if the pore water had become saturated with methane.

3. Numerical models

This study employed numerical modeling to test the hypothesis that the present hydrate accumulation observed at the Shenhu site dynamically evolved from an ancient hydrate deposit, as fluid flow varied over time under different tectonic conditions. The model integrates geological constraints, sedimentation processes, and time-dependent fluid migration to reproduce the observed hydrate distribution.

3.1. Model formulas

Sedimentation rate and fluid-flow rate are crucial factors for hydrate accumulation in marine sediments and should therefore be resolved preferentially in numerical modeling. The model used to simulate gas-hydrate accumulation in the Shenhu area consists of three main components: (1) Calculating sedimentation rate, (2) calculating water-flow rate, and (3) simulating hydrate formation using the mass-balance equation for methane.

3.2. Model assumptions

This study assumed that methane is transported by aqueous advection and diffusion. Hydrate forms only within the gas-hydrate stability zone (GHSZ) when methane concentration in pore water exceeds methane solubility as dictated by hydrate–water equilibrium. Consequently, the hydrate-accumulation rate is proportional to the gradient in L+H CH_4 solubility and the water-flow rate. A larger aqueous-flow rate results in a greater hydrate-accumulation rate.

This study do not account for the recycling of free gas released from dissociated hydrates during continued sedimentation. The progressive burial of gas hydrates across the hydrate-stability boundary would dissociate hydrates into free gas and water. The free gas generated would migrate upward under buoyancy and recrystallize as new hydrate at the base of the newly established hydrate stability field. This model does not consider the effect of recycled gas; the dissociated free gas is assumed to remain trapped in pores below the GHSZ.

This study assume that the water-flow rate before 1.5 Ma, driven by tectonic activity, was higher than that after 1.5 Ma, as the post–1.5 Ma sediments are fine-grained and less fractured (Wu NY et al., 2009).

Here the authors use numerical modeling to test the hypothesis that the present hydrate accumulation observed at the Shenhu site has dynamically evolved from an “ancient” hydrate deposit, considering that fluid flow varied temporally with tectonic events. The model proposed here comprises three stages as shown in Fig. 4.

(i) Stage 1: Before 1.5 Ma, the fast fluid flow in the fractured sediments led to the development of a rapid “ancient” hydrate accumulation in the GHSZ (Figs. 4a, d). At this stage, the top of the hydrate-occurrence zone was pushed upward, i.e., close to the seafloor, because water advection was sufficiently strong to counteract the diffusive loss of methane near the seafloor (Xu WY and Ruppel C, 1999);

(ii) Stage 2: The water-flow rate decreased after 1.5 Ma because the Pleistocene sediments are fine-grained and less fractured. The reduced flow rate caused several dynamic effects in the gas-hydrate system. First, the lower flow rate may have decreased the amount of heat supplied to the sediment column by advective heat transport, thereby cooling the sediments and increasing the thickness of the GHSZ (Fig. 4b). Second, the temperature drop may have increased the L+G methane solubility required to form the free-gas phase below the GHSZ, which could have delayed gas exsolution from the aqueous phase. Third, the reduced flow rate would limit the amount of methane supplied to near-surface sediments, where pore water is undersaturated with methane and hydrates cannot form. As the “ancient” gas hydrates formed at Stage 1 were progressively buried below the boundary of the GHSZ, they dissociated into free gas and water. A free-gas zone developed below the GHSZ (shaded area in Fig. 4e).

(iii) Stage 3: At this stage, more gas hydrates accumulated during Stage 1 were buried out of the hydrate-stability field, and a thicker free-gas zone developed. However, only a small amount of “new” hydrate accumulated in the young sediments due to the low post–1.5 Ma water-flow rate (Fig. 4c). As a result, the total amount of gas hydrate in the system decreased over time because the rate at which “ancient” hydrates in old sediments were buried out of the hydrate-stability field exceeded the rate at which “new” hydrates formed in young sediments (Fig. 4f). The burial rate of “ancient” hydrates out of the GHSZ, v_{ah}, can be approximated by the following equation (Eq. 1):

$$v_{ah} = v_s \varphi S_h \tag{1}$$

where v_s, φ, and S_h denote the sedimentation rate, sediment porosity, and hydrate saturation, respectively, at the base of GHSZ. The total growth rate of hydrates in the young sediments, v_h, can be approximated by integrating the

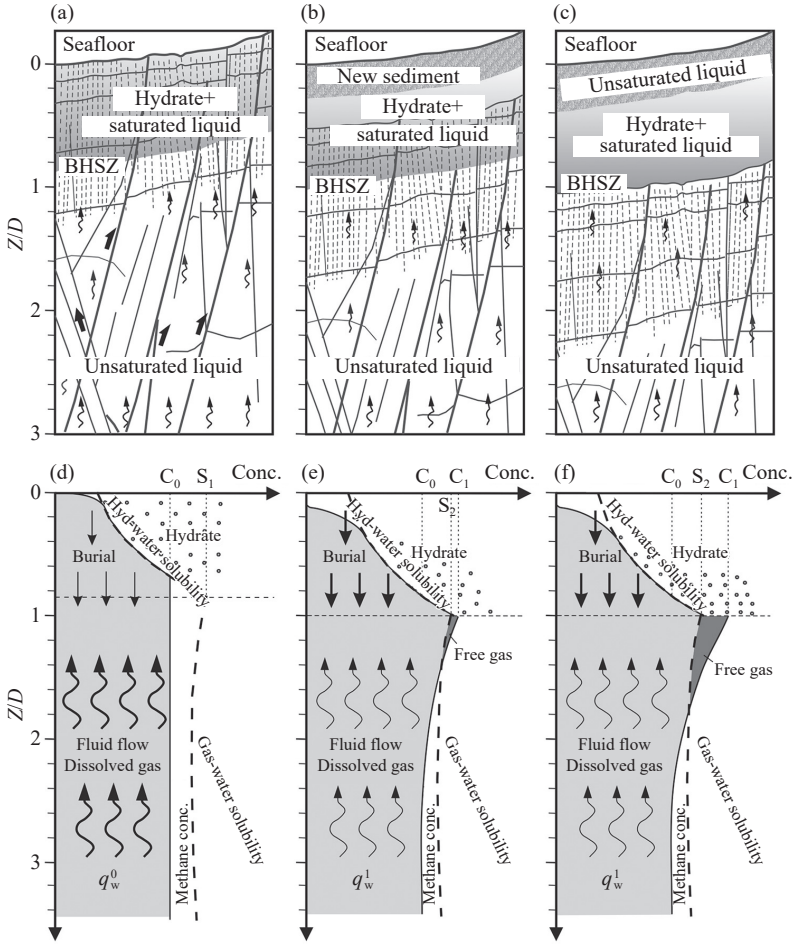

Fig. 4. Conceptual model of gas hydrate accumulation and development in the Shenhu area (after Haacke R et al., 2008). a, b, c–Schematic illustration of the geologic evolution of the sediment and gas hydrate at the three stages; d, e, f–thermodynamic evolution of hydrate accumulation at the three stages. BHSZ–Base of hydrate stability zone.

following equation over the depth interval of GHSZ (Eq. 2):

$$v_{\mathrm{h}} = \int_{z=D}^{0} (v_{\mathrm{w}} \cdot \nabla S_{\mathrm{m}}) dz \tag{2}$$

where v_{w} is the water flow rate, S_{m} is the methane solubility, and D is the depth to the base of GHSZ.

3.3. Numerical-model workflow

The complete modeling procedure is summarized in Fig. 5. The framework consists of three coupled modules: (1) Sediment compaction and porosity evolution; (2) fluid flow and solute transport; and (3) hydrate formation governed by methane solubility and phase equilibrium within the GHSZ. Boundary conditions, parameter inputs, and representative outputs (methane concentration, hydrate saturation, temperature) are also outlined. This schematic provides a transparent overview of how geological data are translated into quantitative simulations of hydrate dynamics.

4. Mathematical model

4.1. Sedimentation rate

At the geologic time scale, sedimentation leads to sediment compaction, where sediment porosity is related to vertical effective stress in the compaction theory (Gutierrez M and Wangen M, 2005). For one-dimensional compaction, porosity (φ) can be written as a function of the effective stress or burial depth. In this model, porosity is assumed to be in a steady state and form (Eq. 3; Athy L, 1930; Haacke R et al., 2008):

$$\varphi = \varphi_0 e^{-z/\lambda} \tag{3}$$

where λ is the compaction length, and φ_0 is the seabed porosity. The compaction length reflects the physical properties of seabed sediments, and its value can be fitted from porosity values measured from core samples.

The porosity-depth relation, along with mass balances for sediments, provides an expression for the sediment flux (Xu WY and Ruppel C, 1999; Davie M and Buffett B, 2001). The sediment balance (Eq. 4) can be written as:

$$\frac{\partial}{\partial t}(1-\varphi)\rho_s + \nabla \cdot \left[v_s \rho_s (1-\varphi)\right] = 0 \tag{4}$$

where ρ_{s} is the sediment density, and v_{s} is the sediment velocity. Assuming a steady state leads to an invariant sediment flux (U_{s}) with depth, which can be related to the sedimentation rate (S) as the boundary condition imposed at

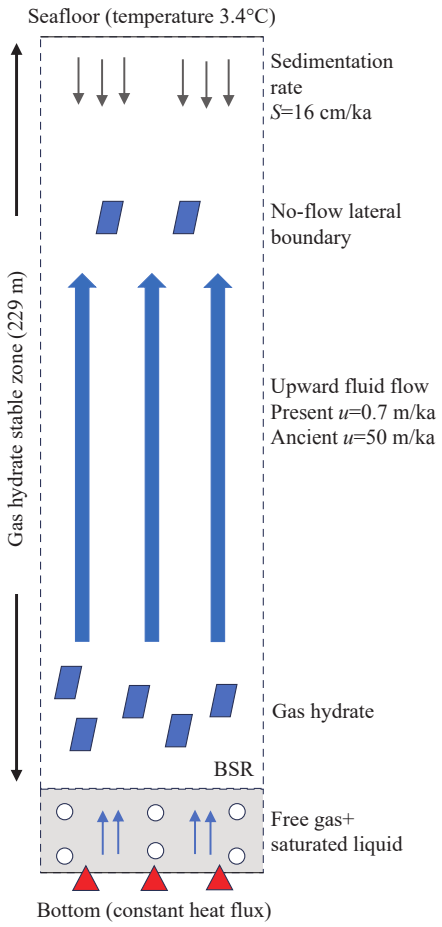

Fig. 5. Schematic workflow of the numerical-modeling framework used in this study, showing the coupling among sedimentation, fluid flow, heat transfer, and hydrate formation. The diagram summarizes boundary conditions, input parameters, and key model outputs.

the seafloor. Because porosity (φ) is in steady state along the vertical direction and sediment density (ρ_s) can be taken as a constant, the term $[\rho_s(1-\varphi)]$ in the equation is invariant over time at a specific depth, which drives the second term $\nabla\cdot\left[v_s\rho_s(1-\varphi)\right]=0$. The sediment density is assumed to be constant in this model; an equation of invariant depositional flux (Eq. 5) is thus drawn as per Bhatnagar G et al. (2007):

$$U_s = v_s(1-\varphi) = S(1-\varphi_0) \tag{5}$$

Here, U_s is the invariant sediment flux, and S is the sediment depositional rate at the seafloor. According to Eq. 5, sedimentation rate beneath the seafloor can be calculated as a function of porosity.

The one-dimensional profiles of porosity and sedimentation rate derived from core and log data at site SH2 are shown in Fig. 6. The Athy-type compaction curve fitted to measured porosities validates the assumed steady-state compaction relationship, and the calculated sedimentation velocity agrees with field constraints.

Permeability variations were parameterized as a function of porosity using an empirical relationship conceptually modified from Han H (2023), as shown in Fig. 7. This conceptual model captures the contrast between fine-grained (D = 2 μm) and coarse-grained (D = 250 μm) sediments, illustrating the strong control of grain size and compaction on fluid flow. The relationship follows a Kozeny–Carman–type formulation of the form (Eq. 6):

$$k = k_0\left(\frac{\varphi}{\varphi_0}\right)^m \tag{6}$$

where k_0 is the reference permeability, φ_0 is the initial porosity at the seafloor, and m is an empirical exponent derived from literature data. Although simplified, this parameterization serves as a conceptual framework for linking porosity reduction due to compaction with permeability

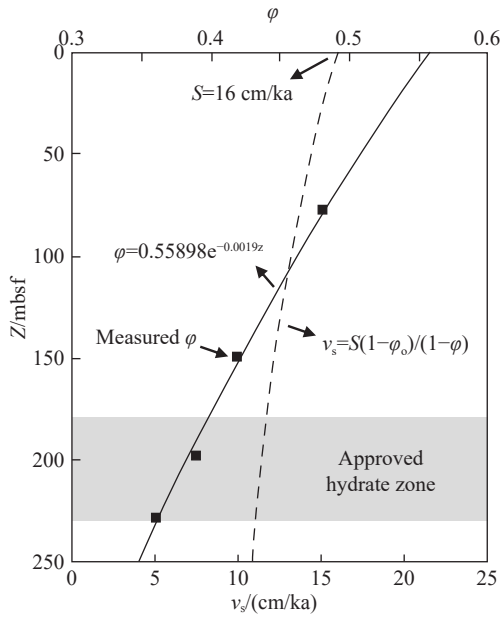

Fig. 6. One-dimensional profiles of porosity and sedimentation rate at site SH2. The solid line shows the porosity–depth relationship fitted by an Athy-type compaction law, and the dashed line denotes the vertical sedimentation velocity derived from the invariant depositional flux. The shaded band marks the hydrate-bearing interval constrained by pore-water chloride anomalies and depressurization tests (after Wu NY et al., 2010; Su Z et al., 2012).

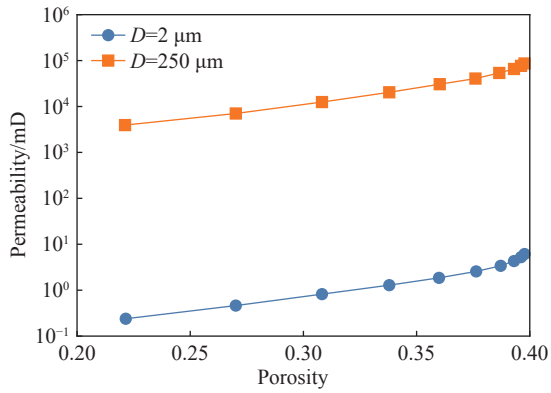

Fig. 7. Porosity–permeability relationship adopted in the model (after Han H, 2023). The empirical curves follow a Kozeny–Carman–type formulation for different mean grain diameters, demonstrating how compaction strongly reduces permeability in fine-grained sediments.

decline in the Shenhu sediments.

4.2. Water flow rate

Anoxic methane oxidation (AMO) in marine sediments is a complex biogeochemical process (Hinrichs K and Boetius A, 2002; Joye S et al., 2004; Treude T et al., 2005). The upward-flowing methane gas is oxidized by the downward diffusing sulfate in shallow depths, leading to a sharp decline in sulfate and methane contents. The AMO mainly occurs at the sulfate-methane interface (SMI) (Hinrichs K and Boetius A, 2002; Joye S et al., 2004; Treude T et al., 2005). In the AMO, methane and sulfate are consumed and transformed to dissolved inorganic carbon (DIC) and hydrogen sulfide (HS^-); the biogeochemical reaction of this processes is: $CH_4 + SO_4^{2-} \rightarrow HCO_3^- + HS^- + H_2O$ (Hinrichs K and Boetius A, 2002; Joye S et al., 2004; Treude T et al., 2005).

Methane concentration at the SMI in the hydrate field in the Shenhu area is close to zero (Wu NY et al., 2010), indicating that the upward migrating methane is almost completely consumed by the sulfate that diffuses downward from seawater. Methane and sulfate reach a reactive equilibrium at the SMI depth. The methane gas dissolved in pore water migrates via convection and diffusion, and the sulfate migrates mainly via diffusion, as indicated by the proportional change. Therefore, the equilibrium equation (Eq. 7) is as follows (Su Z et al., 2012):

$$v_w \rho_f c_m^l - D_m \frac{\partial c_m^l}{\partial z} - D_s \frac{\partial c_s^l}{\partial z} = 0 \tag{7}$$

Eq. 7 shows that the amount of methane migrating upward from deeper layers is equal to the content of downward diffusing sulfate; v_w is the fluid flow rate, ρ_f is the pore fluid density, c_m^l and c_s^l are the concentrations of methane and sulfate in the liquid, respectively, and D_m and D_s are the diffusion coefficients of methane and sulfate in the liquid phase, respectively.

Methane concentration within the hydrate zone is equal to methane solubility. The gradient of methane concentration is very small, and thus, the contribution of methane diffusion to methane transfer can be neglected in the above equation. The water flow rate can be simplified as (Eq. 8):

$$v_w \approx \frac{D_s}{\rho_f c_m^{l,h}} \frac{\partial c_s^l}{\partial z} \tag{8}$$

where $c_m^{l,h}$ represents methane concentration in the hydrate zone, and is equal to methane solubility at the given depth. The water flow rate can be calculated by using the equation if the gradient of sulfate concentration and solubility of methane in the hydrate zone is known.

4.3. Equilibrium formation of hydrates

The distribution of hydrates in submarine sediments is strongly dependent on two *P–T*-dependent equilibrium solubility curves (Liu XL and Flemings P, 2007). These methane-solubility curves define the thickness of the GHSZ. They also provide the methane concentration required for hydrate formation within the GHSZ and thus control the accumulation process of methane hydrates. The model of Duan Z et al. (1992) was used to predict methane solubility under liquid–gas equilibrium, whereas the model of Davie M et al. (2004) was used to predict methane solubility under liquid–hydrate equilibrium.

The mass conservation equation describes the transfer of methane among different phases, and the energy conservation equation explains energy exchange and temperature evolution during hydrate formation. These conservation equations were simplified to analyze hydrate accumulation in the Shenhu area by considering only the liquid and hydrate phases within the GHSZ. The free-gas phase was excluded from the model for simplicity. The gas concentration was set equal to methane solubility at the base of the GHSZ during modeling. The equations indicated that gas-hydrate saturation is a function of seafloor sedimentation rate and water-flow rate (Su Z et al., 2012).

5. Results

The model column was fixed in space relative to the seafloor, while materials were allowed to move through the system. The geological parameters of the hydrate deposit at drilling site SH2 were used in the modeling: Water depth was 1235 m, salinity was 3.34%, bottom-water temperature was 3.4°C, and the average geothermal gradient was about 47°C/km (Zhang HQ et al., 2007; Wu NY et al., 2008, 2009). The sediment age at the base of the hydrate zone was about 1.58 Ma, close to the end of the last tectonic activity that occurred between 2.0 Ma and 1.5 Ma. In a previous study, sediment porosity (Eq. 9) was fitted as:

$$\varphi = 0.55898 e^{-0.0019z} \tag{9}$$

where the depth to the base of the GHSZ was 229 mbsf, the average sedimentation rate at the seafloor was 16 cm/ka, and the current water-flow rate was 0.7 m/ka (Su Z et al., 2012). The simulated domain of the sediment was 250 m in thickness.

5.1. "Ancient hydrate" formation

The sediment in the Shenhu area experienced large-scale tectonic activity followed by the deposition of muddy silt. The hydrates currently observed in these muddy-silt sediments are considered to have developed from "ancient hydrates" formed during the late phase of tectonic activity (Su Z et al., 2012). The water-flow rate undoubtedly experienced complex variations during this period, and it is impractical to determine directly the specific value at which hydrates initially formed. An alternative approach is to determine the saturation of the "ancient hydrates" by repeatedly incorporating different initial hydrate-saturation values into the calculations. The model was then run using the average seafloor depositional rate of 16

cm/ka and the current water-flow rate of 0.7 m/ka. The initial value of "ancient hydrate" saturation can thus be derived by identifying the best match between the simulated saturation curve and the saturation values inferred from chloride anomalies.

This study assumes a uniform hydrate saturation of 20% (S_h^0, the dashed line in Fig. 8) throughout the GHSZ as the model's initial condition at 1.5 Ma. The model was then run with the average sedimentation rate (16 cm/ka) and the current water-flow rate (0.7 m/ka) to simulate the post–1.5 Ma dynamic evolution of the gas-hydrate system at drilling site SH2 (Fig. 8).

The methane concentration is zero above the SMI depth of 26 mbsf, and thus no gas hydrate forms in the shallow sediment below the seafloor (Su Z et al., 2012). The maximum methane concentration is 0.136 mol/L at the base of the GHSZ, indicating the gas content in pore water flowing into the GHSZ. Part of the dissolved gas crystallizes as hydrate within the GHSZ because the methane concentration exceeds methane solubility. Therefore, gas-hydrate saturation changes over time. It decreases from the initial value of 20% and reaches a balance in the upper section. The depth interval of equilibrium hydrate saturation progressively extends downward. The equilibrium hydrate saturation increases with depth and reaches 17% at the base of the GHSZ (the line signed by t_4 in Fig. 8).

Gas-hydrate saturation increases at the base of the GHSZ because of continuous hydrate formation. The maximum hydrate-saturation values at the base of the GHSZ are 0.47 at the evolution time of t_1 (= 1.4 Ma), 0.49 at t_2 (= 1.5 Ma), and 0.50 at t_3 (= 1.6 Ma), which approach the saturation value of 48% derived from the salinity anomaly (Su Z et al., 2012). The hydrate zone indicated by the discrete hydrate-saturation values from chloride (22 m thick) at the bottom of the GHSZ is evidently thinner than that simulated at the evolution time of 1.4 Ma (t_1). It also differs substantially from the modeled distribution at 1.6 Ma (t_3). The discrete saturation values are matched well by the simulation curve at the evolution time of 1.5 Ma (t_2). The time of 1.5 Ma corresponds to the end of the tectonic activities and also matches the sediment age (Su Z et al., 2012).

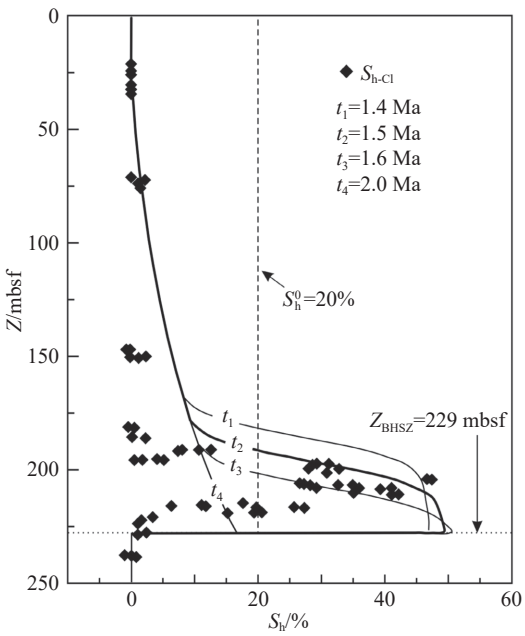

Fig. 8. Gas hydrate saturation calculated at conditions of the initial saturations of 20% (S_h^0) indicating "ancient hydrate", the seafloor sedimentation rate of 16 cm/ka, and water flow rate of 0.7 m/ka. The hydrate saturation derived from chloride, $S_{h\text{-}Cl}$, matched well with the curve calculated at the evolution time of 1.5 Ma (the thick line signed by t_2). The depth to the base of GHSZ is 229 mbsf.

The result indicates that the "ancient hydrate" with 20% saturation formed at the end of the most recent tectonic activity. The hydrate deposit subsequently evolved by inheriting this "ancient hydrate", forming the present hydrate accumulation in the Shenhu area.

5.2. Dynamic gas hydrate accumulation

The modeling results above indicate that hydrates with 20% saturation were formed in the fractured sediment before 1.5 Ma. Thereafter, the "ancient hydrate" underwent a 1.5 Ma evolution under the current sedimentation rate and water-flow rate. The present hydrates in the Shenhu area thus developed by inheriting the "ancient hydrates" with 20% saturation. However, it remains unclear how the "ancient hydrates" formed within the fractured sediment and evolved into the current hydrate deposits.

The water-flow rate in the fractured sediment determined the early hydrate-formation pattern and also influenced the subsequent evolution of the gas-hydrate deposits. A complete evolution sequence of hydrates in fractured sediment without pre-existing hydrate can be generated by repeatedly adjusting the early water-flow rate in the calculations v_w^0. denotes the early water flow rate in the fractured sediment to distinguish v_w^1 of the later water flow rate (0.7 m/ka) in the post-1.5 Ma dynamic evolution of gas hydrate system. This study ran the model at v_w^0 until the average gas hydrate saturation reached 20%, and then adjusted the water flow rate to v_w^1 to represent the dynamic evolution of hydrate deposit in the late period. The sedimentation rate at the seafloor was maintained at 16 cm/ka in the model.

This study assumed an early water flow rate of 50 m/ka to model the hydrate formation in the fractured sediment. The model was then run with v_w^0= 50 m/ka for gas hydrate accumulation in the early period and v_w^1= 0.7 m/ka in the late period. Fig. 9 clearly shows the two distinct stages of gas-hydrate development. In the early stage characterized by rapid water flow, the depth to the base of the GHSZ is 197 mbsf, and gas hydrate grows quickly with an almost uniform saturation across the entire GHSZ, including the sediment beneath the seafloor. The curves t_1 and t_2 represent hydrate growth in the early stage when water flowed rapidly through the fractured sediment. Gas-hydrate saturation is 11% at 20 ka (t_1) and reaches 20% at 40 ka (t_2). The gas hydrate formed in this early period is termed the "ancient hydrate" in the model.

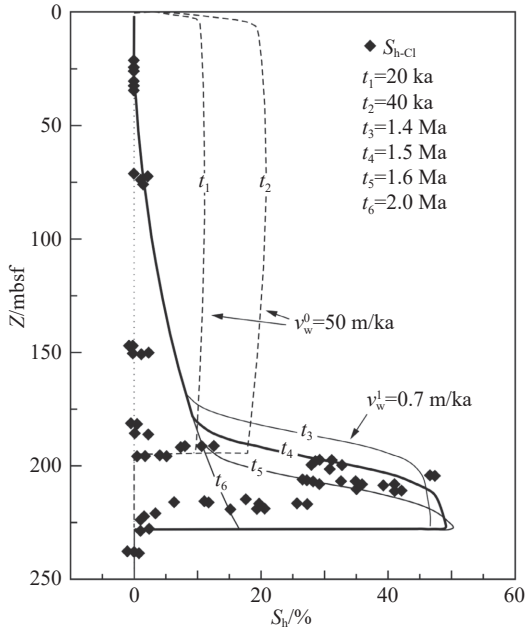

Fig. 9. Dynamic evolution of the hydrate accumulation at site SH2. v_w^0 of water flow in the early stage is 50 m/ka, v_w^1 of water flow in the late stage is 0.7 m/ka. The sedimentation rate at the seafloor is 16 cm/ka. The water flow rate is altered from v_w^0 to v_w^1 upon the average saturation of gas hydrate reaches 20% in the simulation. The dashed lines denote the evolution of gas hydrate in the first stage, and the solid lines indicate the evolution in the second stage. The modeling indicates that the "ancient hydrate" of 20% saturation forms in the fractured sediment within time of 40 ka at the water flow rate of 50 m/ka, and that the hydrate experiences a successive evolution of 1.5 Ma in the late stage at the water flow rate of 0.7 m/ka and then becomes the present hydrate deposit.

Thereafter, the system enters the late period with a low water-flow rate. The gas hydrate deposit develops at the conditions of v_w^1 = 0.7 m/ka and S = 16 cm/ka by inheriting the "ancient hydrate". The curves of t_3–t_6 represent hydrate evolution during the late stage, when the fractured sediment became progressively buried beneath fine-grained, low-permeability sediment. The hydrate evolution during this period exhibits features similar to those described in Fig. 8. The modeled hydrate-saturation curve at 1.5 Ma (t_4) matches well with the discrete hydrate-saturation values derived from chlorinity (Wu NY et al., 2010). The results suggest that the gas-hydrate system underwent a continuous 1.5 Ma evolution after the "ancient hydrate" formed in the fractured sediment and ultimately developed into the present deposit.

The dynamic evolution of gas hydrate accumulation at site SH2 in the Shenhu area was successfully simulated. The modeling results validate the key assumptions of the conceptual model and provide a quantitative description of hydrate evolution. During the first stage, "ancient hydrates" formed within the fractured sediments at the end of tectonic activity, reaching a saturation of approximately 20% in the GHSZ under a rapid water-flow rate of 50 m/ka. In the second stage, the fractured sediments were overlain by low-permeability clayey–silt deposits, and the water-flow rate decreased to 0.7 m/ka. The hydrate system subsequently evolved under these reduced-flow conditions, after approximately 1.5 Ma of development, and produced the hydrate deposits observed today.

The total evolution time of hydrate accumulation at site SH2 is estimated to be about 1.54 Ma, consistent with the termination of the last tectonic event and comparable to the sediment age at the base of the GHSZ (Su Z et al., 2012). These modeling results suggest that gas hydrates in the Shenhu area formed during Late Neogene tectonic activity and underwent a two-stage evolutionary process. The development of hydrates is closely linked to regional tectonism, sedimentation, and geological conditions, consistent with the proposed conceptual model.

5.3. Temperature evolution

The exothermic reaction associated with hydrate formation may cause an increase in sediment temperature within the GHSZ. Fig. 10 shows a temperature elevation of 2°C at 40 ka and a water-flow rate of 50 m/ka, implying that hydrates formed rapidly in the fractured sediment. In the second stage, the water-flow rate decreased to 0.7 m/ka because of the limited permeability resulting from the rapid deposition of fine-grained sediment. The system temperature began to decline and returned to a state similar to the sediment temperature measured *in situ* at drilling site SH2 in the Shenhu area (Wu NY et al., 2010). Heat was also generated during the second stage of hydrate accumulation. However, the thermal regime was moderated and balanced by thermal convection and conduction in this open system. Thus,

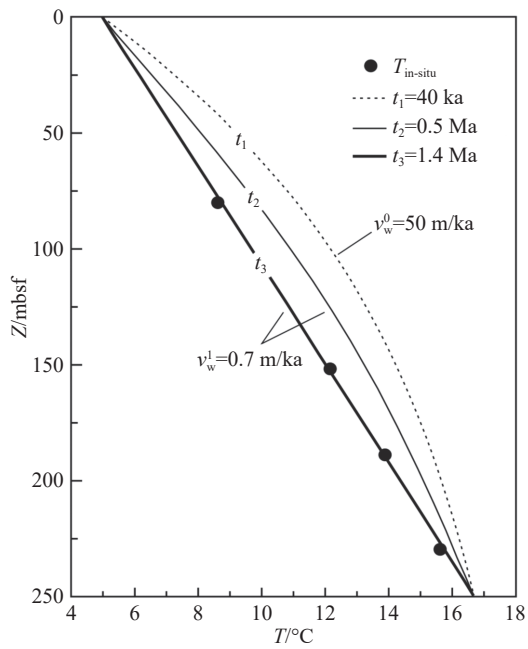

Fig. 10. Temperature of sediments at site SH2 during the dynamic hydrate accumulation. The sediment temperature elevated in the first stage of hydrate formation at a rapid water flow of 50 m/ka (the dashed line signed by t_1), but decreased at the low water flow rate of 0.7 m/ka to the equilibrium state (the lines signed by t_2 and t_3). $T_{in\text{-}situ}$ are the measured temperatures *in-situ* at site SH2 (Wu NY et al., 2010).

sediment temperature decreased and tended toward equilibrium (lines signed by t_2 and t_3 in Fig. 10).

6. Discussion

The dynamic accumulation of methane hydrate in the Shenhu area was investigated using an equilibrium model of hydrate formation controlled by two key parameters: Seafloor sedimentation rate and water-flow rate. This modeling approach can also be applied to clarify hydrate development elsewhere, such as the asymmetrical distribution of hydrates at the Blake Ridge (Paull C et al., 2000). However, the model is still incomplete and extremely simplified (Su Z et al., 2012), and some aspects of the hydrate system require discussion.

The free-gas phase was not included in the model. This simplification made the modeling more tractable and clarified the dynamic evolution within the GHSZ. A limitation of the model is that the buildup of free gas beneath the hydrates is not explicitly represented. Hydrate lifetime in submarine sediments is influenced by sedimentation, which can cause hydrate dissociation and free-gas accumulation below the GHSZ. Previous investigations suggest that a limited amount of free gas may be present in the sediment beneath the hydrates at the drilling site (Zhang W et al., 2007; Su Z et al., 2012). Therefore, some unresolved questions remain, such as: How much free gas was produced beneath the hydrates, how much gas remained in the *in-situ* sediments, and how the free gas was trapped by the hydrate seal?

A small variation in water-flow rate would not significantly affect hydrate growth in fine-grained sediments (Su Z et al., 2012), whereas changes of several orders of magnitude can have substantial impacts on hydrate accumulation. Rapid water flow likely occurred in the fractured sediment generated by faulting. Subsequently, sediment permeability became restricted due to hydrate plugging in the fluid pathway and the rapid burial of fine-grained sediment at the seafloor. The water-flow rate decreased to a low value of 0.7 m/ka based on pore-water geochemistry (Su Z et al., 2012). In this modeling, the water-flow rates were treated as a “sudden change” between the two stages, which may differ from the natural rate of change to some degree.

Methane concentration in the water flowing at the base of the GHSZ was evaluated as equal to methane solubility under the modeled conditions. This assumption led to the result that gas hydrates could form at the base of the GHSZ from the outset as saturated water entered. In reality, methane concentration in pore fluid may be lower than the value used here. In such cases, hydrates may initially form in the upper part of the hydrate zone and then migrate downward due to sedimentation, as previously reported by Bhatnagar G et al. (2007). Water in deeper regions becomes saturated gradually. Subsequently, methane concentration at the base of the GHSZ reaches methane solubility as older gas hydrates migrate toward the lower boundary of the GHSZ.

Although the proposed model successfully reproduces the observed hydrate distribution at site SH2, several simplifying assumptions should be noted.

First, pore-pressure evolution during hydrate formation and burial was not explicitly solved. The effect of pressure variation is implicitly represented through the coupling among porosity, permeability, and compaction. In natural systems, local permeability reduction caused by hydrate growth would increase effective stress and pore pressure, a process qualitatively consistent with the conceptual model used here.

Second, the model does not explicitly simulate the salt-exclusion process associated with hydrate crystallization. However, the modeled hydrate-bearing interval corresponds well with the depth range constrained by measured pore-water chloride anomalies (Fig. 6), suggesting that the salinity-related feedback is reasonably captured at the system scale. The influence of salinity on methane solubility and hydrate stability is implicitly included through the equilibrium equations of Duan Z et al. (1992).

Third, the present one-dimensional model assumes homogeneous sediment properties. In reality, spatial heterogeneity in grain size, permeability, and mineral composition can strongly influence hydrate morphology and growth kinetics. Laboratory and numerical studies have shown that hydrate formation and dissociation often lead to spatially heterogeneous distributions even under controlled conditions (Yin ZY et al., 2018). Field-scale simulations further demonstrate that geological structures such as formation dip and alternating sand–clay layers can modify methane-migration pathways and affect the total hydrate accumulation (Bei KQ et al., 2022). More recently, Ren JJ et al. (2024) showed that clayey–silty sediments promote two-stage hydrate growth, with fine-grained particles forming thin barrier layers that induce stratified and heterogeneous hydrate distributions. These findings support the conceptual interpretation that fine-grained sediments in the Shenhu area restrict upward methane migration and lead to heterogeneous hydrate occurrence.

Despite these simplifications, the model provides a robust first-order framework for understanding the dynamic evolution of ancient and modern hydrate systems in continental-margin settings and can serve as a basis for future two- or three-dimensional studies incorporating explicit pressure, salinity, and heterogeneity effects.

7. Conclusions

The present study investigates the dynamic evolution of gas-hydrate accumulation in the Shenhu area of the northern South China Sea by integrating geological evidence with time-dependent numerical modeling. The key findings and implications are summarized as follows.

(i) Two-stage evolution: The hydrate system at site SH2 evolved through two distinct stages. During the Late Pliocene–Early Pleistocene (2.0–1.5 Ma), intense tectonic activity fractured the sediments and enhanced upward fluid

flow (about 50 m/ka), leading to the rapid formation of "ancient hydrates" with saturations up to 20%. After tectonic quiescence, fine-grained sedimentation reduced permeability and water-flow rate (about 0.7 m/ka), producing the modern hydrate distribution.

(ii) Inheritance of "ancient hydrates": The present hydrate layer is interpreted as the remnant of ancient hydrates that were progressively buried and partially dissociated as the gas-hydrate stability zone (GHSZ) shifted downward over time.

(iii) Controlling factors: The coupled effects of sedimentation rate, permeability evolution, and variable water flow govern the long-term hydrate accumulation and dissociation in the Shenhu area.

(iv) Model implications: The dynamic model successfully reproduces the observed hydrate-saturation profile at site SH2 and highlights the dominant role of temporally varying fluid flow in shaping the hydrate system.

(v) Broader significance: This work provides a conceptual framework for understanding the transition from paleo- to modern hydrate systems in continental-margin settings and offers insights into hydrate resource assessment under changing geological conditions.

CRediT authorship contribution statement

Zheng Su led the conceptualization, methodology design, investigation, formal analysis, and preparation of the original draft, and was responsible for project administration, supervision, and funding acquisition. Yi-fan Wu contributed to data curation, software implementation, validation, figure preparation, and manuscript revision, including assisting with responses to reviewers. Neng-you Wu provided essential resources, senior supervision, and project oversight, and contributed to the review and refinement of the manuscript.

Declaration of competing interest

The authors declare no conflicts of interest.

Acknowledgment

This research was supported by the Guangzhou Marine Geological Survey, the Key Project of Guangdong Provincial Key R & D Program (2023B1111050014), the Youth Promotion Project of the Natural Science Foundation of Guangdong Province (2023A1515030280), the Guangdong Basic and Applied Basic Research Foundation (2023A1515010926), and the Guangzhou Science and Technology Plan Project (2024A04J9876). Additional support was funded by China National Petroleum Corporation (CNPC, 2024DQ02-0107). The authors thank Dr. Xiao-li Liu at Anadarko Petroleum Corporation for stimulating discussions and reviewing the manuscript.

References

Athy L. 1930. Density, porosity, and compaction of sedimentary rocks. AAPG Bull., 14, 1–24. doi: 10.1306/3D93289E-16B1-11D7-8645000102C1865D.

Bei KQ, Tian HL, Xu TF, Li YP, Yin ZY. 2022. Effects of key geological factors in the long-term transport of CH4 and the CH4-hydrate formation behavior with formation dip. Journal of Natural Gas Science and Engineering, 103(24), 104615. doi: 10.1016/j.jngse.2022.104615.

Bhatnagar G, Chapman W, Dickens G, Dugan B, Hirasaki G. 2007. Generalization of gas hydrate distribution and Saturation in marine sediments by scaling of Thermodynamic and transport processes. American Journal of Science, 307, 861–900. doi: 10.2475/06.2007.01.

Biastoch A, Treude T, Rüpke L, Riesbesell U, Roth C, Burwicz E, Park W, Latif M, Büning C, Madec G, Wallmann K. 2011. Rising Arctic Ocean temperatures cause gas hydrate destabilization and ocean acidification. Geophysical Research Letters, 38, L08602. doi: 10.1029/2011GL047222.

Chen C, Jiang T, Kuang ZG, Yang CZ, Zhang C, He YL, Cheng Z, Tian DM, Xiong PF. 2020. Characteristics of gas chimneys and their implications on gas hydrate accumulation in the Shenhu area, northern south China sea. Journal of Natural Gas Science and Engineering, 84, 103629. doi: 10.1016/j.jngse.2020.103629.

Collett T. 2002. Energy resource potential of natural gas hydrates. AAPG Bulletin, 86, 1971–1992. doi: 10.1306/61EEDDD2-173E-11D7-8645000102C1865D.

Davie M, Buffett B. 2001. A numerical model for the formation of gas hydrate below the seafloor. Journal of Geophysical Research: Solid Earth, 106(B1), 497–514. doi: 10.1029/2000JB900363.

Davie M, Buffett B. 2003. Sources of methane for marine gas hydrate: Inferences from a comparison of observations and numerical models. Earth and Planetary Science Letters, 206(1), 51–63. doi: 10.1016/S0012-821X(02)01064-6.

Davie M, Zatsepina O, Buffett B. 2004. Methane solubility in marine hydrate environments. Marine Geology, 203(1), 177–184. doi: 10.1016/S0025-3227(03)00331-1.

Dickens G. 2003. Rethinking the global carbon cycle with a large, dynamic and microbially mediated gas hydrate capacitor. Earth and Planetary Science Letters, 213(3–4), 169–183. doi: 10.1016/S0012-821X(03)00325-X.

Duan Z, Moller N, Greenberg J, Weare J. 1992. The prediction of methane solubility in natural waters to high ionic strength from 0 to 250℃ and from 0 to 1600 bar. Geochimica et Cosmochimica Acta, 56, 1451–1460. doi: 10.1016/0016-7037(92)90215-5.

Fang YX, Lu JA, Liang JQ, Kuang ZG, Cao YC, Chen DF. 2019. Numerical studies of gas hydrate evolution time in Shenhu area in the northern South China Sea. China Geology, 2(1), 49–55. doi: 10.31035/cg2018054.

Guan JA, Liang DQ, Wu NY, Fan SS. 2009. The methane hydrate formation and the resource estimate resulting from free gas migration in seeping seafloor hydrate stability zone. Journal of Asian Earth Sciences, 36(4), 277–288. doi: 10.1016/j.jseaes.2009.05.008.

Gutierrez M, Wangen M. 2005. Modeling of compaction and overpressuring in sedimentary basins. Marine and Petroleum Geology 22(2), 351–363. doi: 10.1016/j.marpetgeo.2005.01.003.

Haacke R, Westbrook G, Riley M. 2008. Controls on the formation and stability of gas hydrate-related bottom-simulating reflectors (BSRs): A case study from the west Svalbard continental slope. Journal of Geophysical Research: Solid Earth, 113(B5), 1–17. doi: 10.1029/2007JB005200.

Han H. 2023. Study on Pore Permeation Characteristics of Gas Hydrate Reservoir in the Shenhu Sea, South China Sea. Beijing, master's thesis, China University of Petroleum, 1–59 (in Chinese with English abstract). doi: 10.27643/d.cnki.gsybu.2023.000162.

Hinrichs KU, Boetius A. 2002. The Anaerobic Oxidation of Methane: New Insights in Microbial Ecology and Biogeochemistry. In: Wefer G, Billett D, Hebbeln D, Jørgensen BB, Schlüter M, van Weering

TCE (eds). Ocean Margin Systems. Springer, Berlin, Heidelberg, 457–477. doi: 10.1007/978-3-662-05127-6_28.

He LJ, Lei XL, Zhang Y. 2011. Numerical modeling of gas hydrate accumulation in the marine sediments of Shenhu Area, Northern South China Sea. Chinese Journal of Geophysics, 54(5), 128–129 (in Chinese with English abstract). doi: 10.1002/cjg2.1612.

Hu GW, Bu QT, Lu WJ, Wang JS, Chen J, Li Q, Gong JM, Sun JY, Wu NT. 2021. A comparative study on natural gas hydrate accumulation models at active and passive continental margins. Natural Gas Industry B, 8(5), 115–127. doi: 10.1016/j.ngib.2021.03.001.

Jin JP, Wang XJ, Guo YQ, Li J, Li YP, Zhang X, Qian J, Sun LY. 2020. Geological controls on the occurrence of recently formed highly concentrated gas hydrate accumulations in the Shenhu area, South China Sea. Marine and Petroleum Geology, 116(7), 104294. doi: 10.1016/j.marpetgeo.2020.104294.

Joye S, Boetius A, Orcutt B, Montoya J, Schulz H, Erickson M, Lugo S. 2004. The anaerobic oxidation of methane and sulfate reduction in sediments from Gulf Mexico cold seeps. Chemical Geology, 205(3), 219–238. doi: 10.1016/j.chemgeo.2003.12.019.

Kuang ZG, Guo YQ. 2011. The sedimentary facies and gas hydrate accumulation models since Neogene of Shenhu Sea area, Northern South China Sea. Earth Science-Journal of China University of Geosciences, 36(5), 914–920 (in Chinese with English abstract). doi: 10.3799/dqkx.2011.096.

Liu XL, Flemings P. 2007. Dynamic multiphase flow model of hydrate formation in marine sediments. Journal of Geophysical Research, 112 (B3), B03101. doi: 10.1029/2005JB004227.

Lunt D, Ridgwell A, Sluijs A, Zachos J, Hunter S, Haywood A. 2011. A model for orbital pacing of methane hydrate destabilization during the Palaeogene. Nature Geoscience, 4(11), 775–778. doi: 10.1038/ngeo1266.

McDonnell S, Max M, Cherkis N, Czarnecki M. 2000. Tectono-sedimentary controls on the likelihood of gas hydrate occurrence near Taiwan. Marine and Petroleum Geology, 17(8), 929–936. doi: 10.1016/S0264-8172(00)00023-4.

Milkov A. 2004. Global estimates of hydrate-bound gas in marine sediments: How much is really out there? Earth-Science Reviews, 66(3), 183–197. doi: 10.1016/j.earscirev.2003.11.002.

Paull C, Matsumoto R, Wallace P, Dillon W. 2000. Proceedings ODP Scientific Results 164: College Station, TX (Ocean Drilling Program). doi: 10.2973/odp.proc.sr.164.204.2000.

Piñero E, Marquardt M, Hensen C, Haeckel M, Wallmann K. 2012. Estimation of the global inventory of methane hydrates in marine sediments using transfer functions. Biogeosciences, 10(2), 55–975. doi: 10.5194/bg-10-959-2013.

Prell W, Wang PX, Blum P, 2000. Ocean Drilling Program Leg 184 Scientific Prospectus South China Sea, site 1144, 184. In: Wang PX, Prell W, Blum P. Proceedings of the Ocean Drilling Program, Initial Reports, Ocean Drilling Program, College Station, TX, 1–97. https://www-odp.tamu.edu/publications/prosp/184_prs/184prosp.pdf

Ren JJ, Yin ZY, Lu HF, Xu CL, Kuang ZG, Deng W, Liu YT, Linga P. 2024. Effects of South China Sea clayey–silty sediments on the kinetics and morphology of CH_4 hydrate: Implications for energy recovery. Applied Energy, 367, 123399. doi: 10.1016/j.apenergy.2024.123399.

Sloan ED, Koh CA. 2008. Clathrate Hydrates of Natural Gases, 3rd ed. Boca Raton, CRC Press, 1–752. doi: 10.1201/9781420008494.

Su Z, Cao YC, Wu NY, Chen DF, Yang SX, Wang HB. 2012. Numerical investigation on methane hydrate accumulation in Shenhu Area, northern continental slope of South China Sea. Marine and Petroleum Geology, 38(1), 158–165. doi: 10.1016/j.marpetgeo.2012.06.005.

Sultan N, Cochonat P, Foucher J, Mienert J. 2004. Effect of gas hydrates melting on seafloor slope instability. Marine Geology, 213(1–4), 379–401. doi: 10.1016/j.margeo.2004.10.015.

Treude T, Niggemann J, Kallmeyer J, Jørgensen B. 2005. Anaerobic oxidation of methane and sulfate reduction along the Chilean continental margin. Geochimica et Cosmochimica Acta, 69(11), 2767–2779. doi: 10.1016/j.gca.2005.01.002.

Wu NY, Yang SX, Zhang HQ, Liang JQ, Wang HB, Su X, Fu SY. 2008. Preliminary discussion on gas hydrate reservoir system of Shenhu Area, North Slope of South China Sea. Proceedings of the 6th International Conference on Gas Hydrates (ICGH 2008), 5700, Vancouver, British Columbia, Canada, 6–10 July 2008. doi: 10.14288/1.0041054.

Wu NY, Yang SX, Wang HB, Liang JQ. 2009. Gas-bearing fluid influx sub-system for gas hydrate geological system in Shenhu Area, Northern South China Sea, Chinese Journal of Geophysics, 52(6), 1641–1650 (in Chinese with English abstract). doi: 10.3969/j.issn.0001-5733.2009.06.027.

Wu NY, Yang SX, Zhang HQ, Liang JQ, Wang HB, Lu JA. 2010. Gas Hydrate System of Shenhu Area, Northern South China Sea: Wire-line Logging, Geochemical Results and Preliminary Resources Estimates, OTC 20485, 2010 Offshore Technology Conference, Houston, Texas, USA, 3–6 May 2010. doi: 10.4043/20485-MS.

Xu WY, Ruppel C. 1999. Predicting the occurrence, distribution, and evolution of methane gas hydrate in porous marine sediments. Journal of Geophysical Research: Solid Earth, 104(B3), 5081–5096. doi: 10.1029/1998JB900092.

Xu WY. 2004. Modeling dynamic marine gas hydrate systems. American Mineralogist 89(8), 1271–1279. doi: 10.2138/am-2004-8-916.

Yin ZY, Moridis G, Chong, ZR, Tan HK, Linga P. 2018. Numerical analysis of experimental studies of methane hydrate dissociation induced by depressurization in a sandy porous medium. Applied Energy, 230, 444–459. doi: 10.1016/j.apenergy.2018.08.115.

Zhang HQ, Yang SX, Wu NY, Su X, Melanie H, Peter S, Kelly R, Heather B, Gary H, GMGS-1 Science Team. 2007. Successful and surprising results for China's first gas hydrate drilling expedition. Fire in the Ice (Methane Hydrate Newsletter), 7(3), 6–9. https://www.netl.doe.gov/File%20Library/Research/Oil-Gas/methane%20hydrates/HMNewsFall07.pdf.

Zhang W, Liang JQ, Wei JG, Lu JA, Su PB, Lin L, Huang W, Guo YQ, Deng W, Yang XL, Wan ZF. 2020. Geological and geophysical features of and controls on occurrence and accumulation of gas hydrates in the first offshore gas-hydrate production test region in the Shenhu area. Northern South China Sea. Marine and Petroleum Geology, 114, 104191. doi: 10.1016/j.marpetgeo.2019.104191.

Zhu LQ, Wei JG, Wu SG, Zhou XQ, Sun J. 2022. Application of unlabelled big data and deep semi-supervised learning to significantly improve the logging interpretation accuracy for deep-sea gas hydrate-bearing sediment reservoirs. Energy Reports, 8(1), 2947–2963. doi: 10.1016/j.egyr.2022.01.139.

Zhu LQ, Sun J, Zhou XQ, Li QP, Fan Q, Wu SL, Wu SG. 2023a. Well logging evaluation of fine-grained hydrate-bearing sediment reservoirs: Considering the effect of clay content. Petroleum Science, 20(2), 879–892. doi: 10.1016/j.petsci.2022.09.018.

Zhu LQ, Wu SG, Zhang CM, Misra S, Zhou XQ, Cai JC. 2023b. Characterization of pore electrical conductivity in porous media by weakly conductive and nonconductive pores. Surveys in Geophysics, 44(3), 877–923. doi: 10.1007/s10712-022-09761-w.

Zhu LQ, Wu SG, Zhou XQ, Cai JC. 2023c. Saturation evaluation for fine-grained sediments. Geoscience Frontiers, 14(4), 101540. doi: 10.1016/j.gsf.2023.101540.

Zhu LQ, Zhou XQ, Sun J, Liu YR, Wang JC, Wu SQ. 2023d. Reservoir classification and log prediction of gas hydrate occurrence in the Qiongdongnan Basin, South China Sea. Frontiers in Marine Science, 10, 1055843. doi: 10.3389/fmars.2023.1055843.